Novel Platinum–Cobalt Alloy Nanoparticles Dispersed on Nitrogen-Doped Graphene as a Cathode Electrocatalyst for PEMFC Applications

*Bhaghavathi P. Vinayan, Rupali Nagar, Natarajan Rajalakshmi, and Sundara Ramaprabhu**

A novel synthesis procedure is devised to obtain nitrogen-doping in hydrogen-exfoliated graphene (HEG) sheets. An anionic polyelectrolyte–conducting polymer duo is used to form a uniform coating of the polymer over graphene sheets. Pyrolysis of graphene coated with polypyrrole, a nitrogen-containing polymer, in an inert environment leads to the incorporation of nitrogen atoms in the graphene network with simultaneous removal of the polymer. These nitrogen-doped graphene (N-HEG) sheets are used as catalyst support for dispersing platinum and platinum–cobalt alloy nanoparticles synthesized by the modified-polyol reduction method, yielding a uniform dispersion of the catalyst nanoparticles. Compared to commercial Pt/C electrocatalyst, Pt–Co/N-HEG cathode electrocatalyst exhibits four times higher power density in proton exchange membrane fuel cells, which is attributed to the excellent dispersion of Pt–Co alloy nanoparticles on the N-HEG support, the alloying effect of Pt–Co, and the high electrocatalytic activity of the N-HEG support. A stability study shows that Pt/N-HEG and Pt–Co/N-HEG cathode electrocatalysts are highly stable in acidic media. The study shows two promising electrocatalysts for proton exchange membrane fuel cells, which on the basis of performance and stability present the possibility of replacing contemporary electrocatalysts.

1. Introduction

Proton exchange membrane fuel cells (PEMFCs) are considered to be promising candidates for mobile and transport applications due to their high energy density, zero emissions, relatively low operating temperature, and minimal corrosion problems. In a PEMFC, however, the slow kinetics of the oxygen reduction reaction (ORR) at the cathode causes a large over-potential that greatly reduces its performance.[1] A highly active cathode electrocatalyst can facilitate the ORR and, therefore, result in a higher efficiency and improved fuel cell performance. Platinum (Pt) is used as the main electrocatalyst in all PEMFC applications since it is sufficiently reactive at low temperatures and easily bonds with the hydrogen and oxygen intermediates to form the final products.[2] The limited resources of Pt and its high cost currently pose a problem for the commercialization of Pt-based PEMFCs. Therefore, the target is to develop an active cathode electrocatalyst with minimum loading of Pt while maximizing the utility of the loaded Pt. In this context, alloying Pt with 3d transition metals (TM), especially Co, Fe, Ni, and Cr, has been demonstrated to increase the ORR activity.[3] In particular, Pt–Co alloys have been found to exhibit enhanced catalytic activity towards the ORR in an atomic ratio of 3:1 to pure Pt.[4] The modified electronic structure of the Pt–TM alloy composite affects the Pt–Pt bond distance resulting in easier adsorption of the oxygen molecules onto alloy nanoparticles.

It is well known that the performance of a fuel cell greatly depends on the composition, shape, size, and dispersion of the catalyst nanoparticles. Catalyst supports play an important role in controlling these properties. A good catalyst support material should have: i) a high surface area; ii) strong affinity towards the catalyst particles to immobilize them, while also ensuring their good dispersion; iii) a high electrical conductivity to promote fast electron transfer in redox reactions; and iv) good chemical stability under the operating conditions to maintain a stable catalyst structure. Presently, carbon-supported platinum (Pt/C) is used as the cathode electrocatalyst in PEMFCs.[2] However, during fuel cell operation, electrochemical oxidation of the carbon support results in the detachment of catalyst nanoparticles from the support and their agglomeration, thereby causing a degradation in performance.[5] In the past few years, graphene has emerged as the ideal material for different energy

B. P. Vinayan, Dr. R. Nagar, Dr. S. Ramaprabhu
Alternative Energy and Nanotechnology Laboratory (AENL)
Nano Functional Materials Technology Centre (NFMTC)
Department of Physics, IITM, Chennai 600036, India
E-mail: ramp@iitm.ac.in
Dr. N. Rajalakshmi
Centre for Fuel Cell Technology
International Advanced Research Centre for Powder Metallurgy and New Materials
ARCI, IIT Madras Research Park
Taramani, Chennai 600 113, India

DOI: 10.1002/adfm.201102544

applications such as fuel cells, Li-ion batteries, supercapacitors, and solar cells because of its large thermal conductivity, high surface area, high mechanical stabilty, and excellent electronic conductivity.[6]

Chemical modification of the inert surface of graphene sheets is necessary for the uniform dispersion of electrocatalyst nanoparticles. Currently, chemical modification by methods including acid oxidation,[7] ionic liquid (IL) linking,[8] and plasma treatment[9] is employed for the purpose. These procedures may cause a partial destruction of the structure of graphene, thereby adversely affecting its novel properties, like an extremely high surface area and high electrical conductivity. The reported Pt–graphene electrocatalysts synthesized by various chemical methods suffer from these problems and hence exhibit low PEMFC performances. This can be compensated by introducing chemically active sites into the graphene network by nitrogen doping. Nitrogen doping of graphene can promote i) faster nucleation and growth kinetics of catalyst nanoparticles leading to their small size and uniform dispersion, ii) increased support/catalyst chemical binding, resulting in enhanced durability, and iii) catalyst nanoparticle electronic structure modification, which enhances intrinsic catalytic activity.[10] In addition, nitrogen-doping of graphene increases its conductivity by raising the Fermi level towards the conduction band.[11] Recently Qu et al. reported that nitrogen-doped graphene itself can act as an efficient metal-free electrocatalyst for the ORR.[12] Therefore, it is crucial to explore the application of nitrogen-doped graphene along with Pt–TM alloys to address the aspect of ORR activity in the field of PEMFCs.

Here, we have attempted to investigate the synergistic effect of a nitrogen-doped graphene support and Pt–Co-based alloy nanoparticles for attaining better PEMFC performance. The necessity to efficiently dope the graphene sheets with nitrogen while averting their agglomeration during wet-chemical synthesis has been emphasized. Initially, an anionic polyelectrolyte is used to distribute negative charges over the surface of hydrogen exfoliated graphene (HEG). The polypyrrole, a cationic nitrogen containing polymer, is then added, which forms a uniform coating over the negatively charged surface of HEG followed by pyrolysis under an inert environment that causes nitrogen atoms to be doped in the graphene network. The Pt and Pt–Co alloy nanoparticles are uniformly dispersed over nitrogen-doped graphene and their electrocatalytic activity towards the ORR has been evaluated by full cell measurements along with stability tests. The results suggest that nitrogen-doped graphene along with Pt–Co alloy nanoparticles have great potential as advanced electrocatalysts for the ORR in PEMFCs.

2. Results and Discussion

The methodology followed here to introduce nitrogen doping in HEG sheets includes two steps: i) uniform coating of conductive polymer (polypyrrole, PPy, in the present case) over graphene surface and ii) pyrolysis of this conductive polymer coated graphene composite in an inert gas atmosphere. To achieve a uniform coating of PPy over graphene, the positive surface charge property of the polymer was utilized. For this, HEG was first treated with an anionic polyelectrolyte poly(sodium

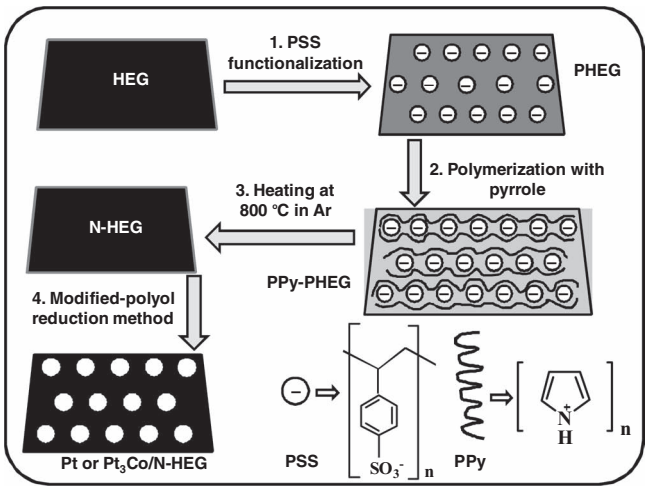

Scheme 1. Schematic illustration of the synthesis procedure of Pt/N-HEG or Pt_3Co/N-HEG.

4-styrenesulfonate) (PSS). The PSS bears negatively charged sulfonate groups (see **Scheme 1**) that readily distributes negative charges all over the graphene sheets (PHEG). This distribution of negative charges over graphene surface, in fact, also avoids their restacking, a problem often encountered in synthesizing graphene nanocomposites that follow a solution-based approach. On chemical polymerization, the negatively charged sulfonate groups of PSS attract the positively charged nitrogen atoms of PPy resulting in a uniform coating of polypyrrole over graphene sheets (PPy–PHEG). Therefore, polyelectrolytes can be used as "guides" at the nanoscale to form uniform coating of conducting polymers on substrates like graphene, as demonstrated here. Scheme 1 summarizes the methodology for synthesizing the platinum and platinum–cobalt alloy nanoparticle decorated nitrogen-doped graphene. The detailed experimental procedure is described in the Experimental Section.

Structural characterization of the specimens was carried out using powder X-ray diffraction (XRD). **Figure 1** shows the XRD patterns of: a) HEG, b) nitrogen-doped graphene (N-HEG), c) platinum-decorated N-HEG (Pt/N-HEG), and d) platinum–cobalt alloy decorated N-HEG (Pt_3Co/N-HEG). In the case of HEG, exfoliation of graphite oxide (GO) with hydrogen at around 200 °C results in a broad peak ranging from 2θ of 14° to 30° suggesting the presence of only a short-range order, which is a typical characteristic of stacked layers of graphene. The interlayer spacing was observed to be 0.37 nm for HEG, 0.34 nm for initial graphite powder and 0.84 nm for the case of graphite oxide (see Figure S1 in the Supporting Information). This increase of *d*-spacing of HEG as compared to graphite suggests loosening of graphene layers along the *c*-axis, while a decrease as compared to graphite oxide indicates removal of oxygen and water from its layers during exfoliation. Similar to HEG, a broad peak ranging from 17° to 30° corresponds to the (002) graphitic plane, indicating the amorphous nature of the stacked layers of nitrogen-doped graphene (Figure 1b). The XRD patterns of Pt/N-HEG and Pt_3Co/N-HEG depicted in Figure 1c,d, respectively, show the presence of (111), (200), (220), and (311) peaks of Pt, which crystallizes in the fcc crystal

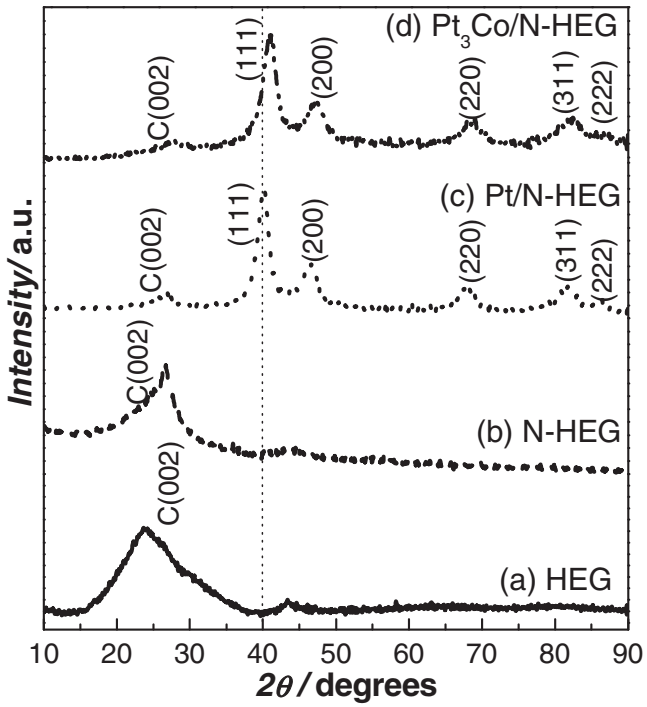

Figure 1. X-ray diffractograms of: a) HEG, b) N-HEG, c) Pt/N-HEG, and d) Pt_3Co/N-HEG.

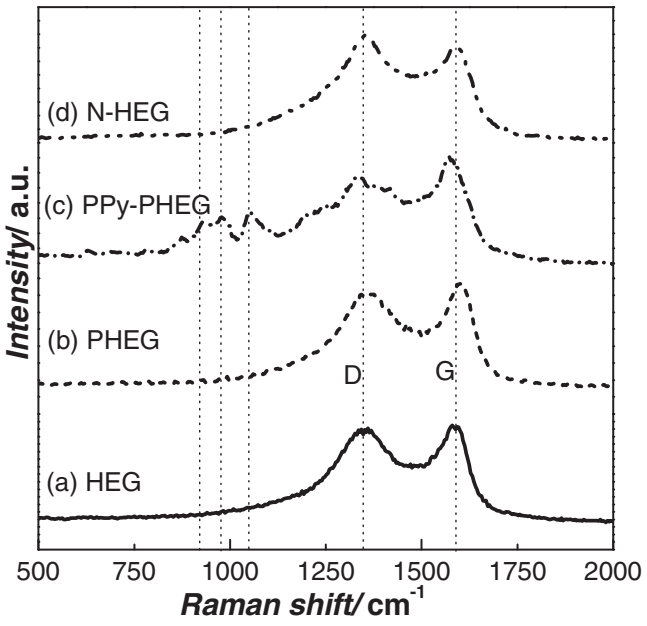

Figure 2. Raman spectra of: a) HEG, b) PHEG, c) PPy–PHEG, and d) N-HEG. The position of the G and D bands has been indicated.

structure along with the C(002) peak. In the case of the Pt_3Co/N-HEG sample, the Pt peaks were observed to shift to higher angles suggesting lattice contraction as compared to pure Pt. This lattice contraction may result when the larger Pt atoms get substituted by smaller Co atoms in the Pt–Co specimen.[13] Interestingly, the signature peaks of cobalt metal or its oxides were not observed for the binary Pt–Co catalyst. These results indicate that Pt and Co species in the Pt–Co catalysts were alloyed together. The X-ray diffractograms of graphite, graphite oxide, PPy, and PPy-PHEG are shown in Figure S1 in the Supporting Information.

Figure 2 shows the Raman spectra of a) HEG, b) PHEG, c) PPy–PHEG, and d) N-HEG. In the case of HEG, a broad G band at 1592 cm^{-1} and D band at 1360 cm^{-1} of comparable intensity showed the presence of defects within the sample. The ratio between the intensities of the D and G bands (I_D/I_G) is used to predict the presence of defects within the samples and has been tabulated in Table S1 in the Supporting Information. The intensity ratio of the D to the G band slightly decreased in PHEG, suggesting coverage of the defect sites of graphene by the PSS polyelectrolyte chains. In the case of PPy–PHEG (Figure 2c), the presence of the additional peaks at 1052, 979, and 927 cm^{-1} along with graphene peaks (G and D band) indicate the coating of the polymer PPy on the graphene surface.[1a] The absence of these peaks in N-HEG (Figure 2d) confirmed that all PPy was removed from the graphene surface after pyrolysis. The increase in the intensity of D band in N-HEG (Figure 2d) confirmed the nitrogen doping, as nitrogen atoms in the graphene network act as defect sites. These sites are, in fact, favourable for nanoparticle dispersion as they act as anchoring sites for metal nanoparticles on subsequent modified-polyol reduction treatment.[9] The formation of surface layer of PPy on PSS functionalized graphene and its removal on heating at high temperature was also supported by Fourier transform infrared (FTIR) spectroscopy, discussed and depicted in Figure S2 in the Supporting Information.

The morphology of the samples was studied using scanning and transmission electron miscroscopy (SEM and TEM). **Figure 3** shows the SEM and TEM images of HEG (a,d), PPy–PHEG (b,e), and N-HEG (c,f) specimens, respectively. The wrinkled morphology of the hydrogen-exfoliated graphene is seen clearly in the TEM image (Figure 3d). The uniform coating of the PPy polymer over the surface of PHEG resulted in an increase in the thickness of the graphene layers, as is evident from the SEM and TEM images of PPy–PHEG (Figure 3b,e). The electrostatic interaction between positively charged PPy and negatively charged graphene surface is responsible for the uniform coating of PPy over PHEG, as discussed earlier. TEM and SEM images of N-HEG (Figure 3c,f) showed well-separated sheets that again indicate the removal of PPy after pyrolysis. Insets in Figure 3d–f present the electron diffraction patterns (DPs) for HEG, PPy-PHEG, and N-HEG, respectively. In all three specimens, the presence of some brighter arcs may be attributed to the presence of large size crystallites of graphene sheets (4–5 layers stacked together along the (002) plane, as observed from XRD analysis) along with fainter rings that indicate their amorphous nature. In case of PPy–PHEG (inset in Figure 3e), diffused rings are visible. This may be attributed to the polymer coating over the surface of graphene sheets.

Figure 4 shows SEM and TEM images of Pt/N-HEG (a,c), and Pt_3Co/N-HEG (b,d). A uniform size distribution of Pt and Pt_3Co nanoparticles over the surface of nitrogen-doped graphene with a good dispersion was observed from the SEM

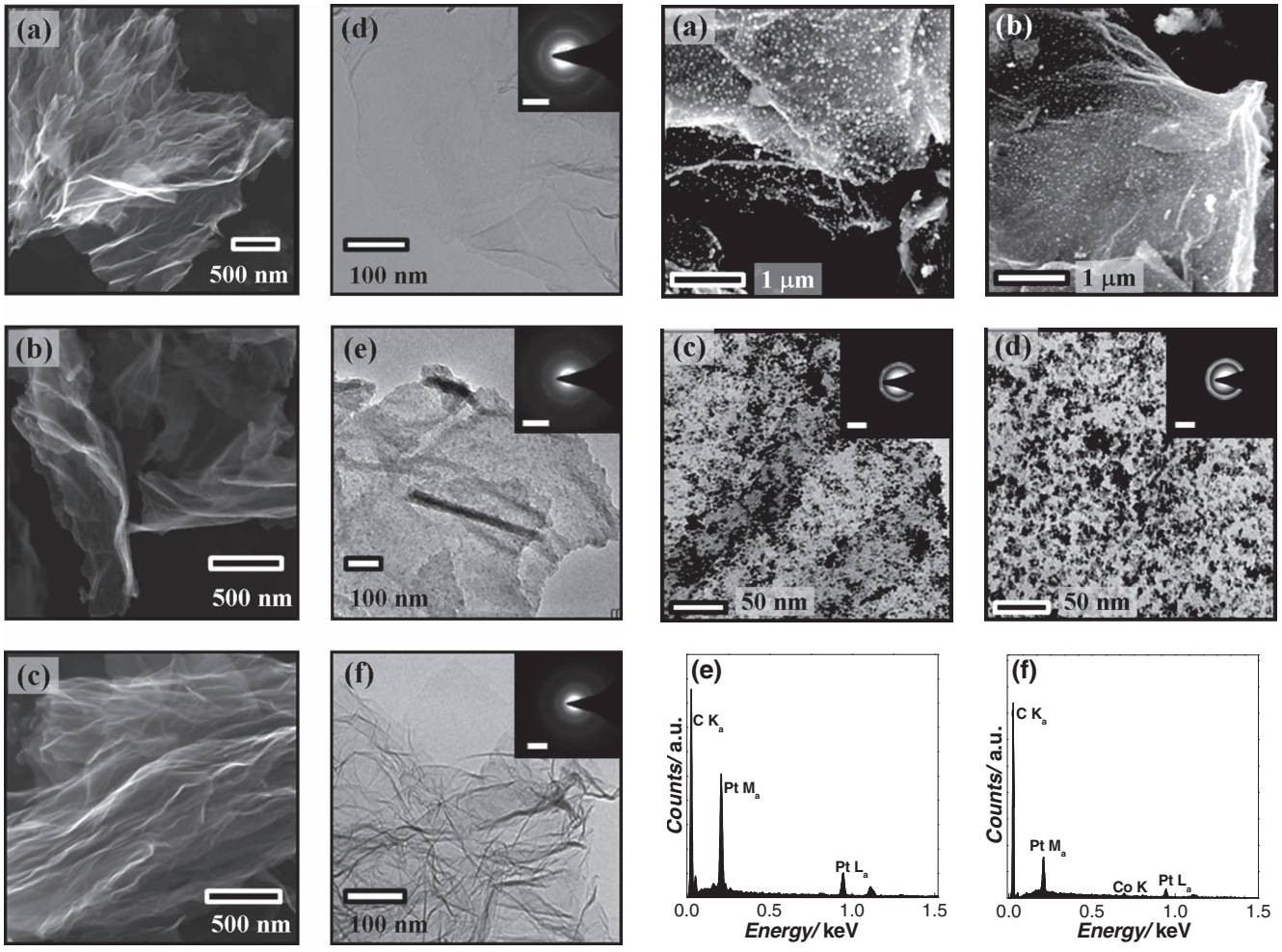

Figure 3. SEM and TEM images of HEG (a,d), PPy–PHEG (b,e), and, N-HEG (c,f). Insets in (d,e,f) show the electron diffraction patterns of HEG, PPy-PHEG, and N-HEG, respectively. The scale bars correspond to 5 nm^{-1}.

Figure 4. SEM and TEM images of Pt/N-HEG (a,c) and Pt_3Co/N-HEG (b,d). Insets in (c,d) show the electron diffraction patterns of Pt/N-HEG and Pt_3Co/N-HEG. The scale bars correspond to 5 nm^{-1}. EDX spectra of Pt/N-HEG (e), and, Pt_3Co/N-HEG (f).

and TEM images (Figure 4a–d). From the analysis of TEM images, the average Pt and Pt_3Co nanoparticle sizes were estimated to be about 2.6 ± 0.4 nm and 2.3 ± 0.5 nm. The size distribution of the particles in the specimens is shown as Figure S3 in the Supporting Information. The particle size of Pt_3Co nanoparticles was smaller than that of the mean size determined for pure Pt nanoparticles. This is consistent with earlier conclusions on the impact of differences in nucleation rate on mean particle size.[13b] The N-doping over graphene surface helped in obtaining a uniform dispersion and optimum particle size of Pt and Pt_3Co alloy nanoparticles. Insets of Figure 4c,d show the DPs of Pt/N-HEG and Pt_3Co/N-HEG samples. The presence of spots in the DPs indicated that the samples had a polycrystalline nature. These spots were indexed as the Pt(111) and Pt(200) planes. The energy dispersive X-ray (EDX) spectra of Pt/N-HEG and Pt_3Co/N-HEG showed 29.6% and 29.2% of metal loading within the electrocatalysts (Figure 4e,f). Also, the EDX spectrum of Pt_3Co/N-HEG shows an atomic ratio of 3:1 for Pt/Co.

The bonding configurations of nitrogen atoms and Pt or Pt–Co alloy nanoparticles in the specimens were characterized by X-ray photoelectron spectroscopy (XPS), as shown in **Figure 5**. The high-resolution N1s spectrum is shown in Figure 5a. The N1s spectrum of N-HEG was deconvoluted into four peaks at 398, 400, 401, and 402.2 eV. The peaks with lower binding energy located at about 398 and 400 eV, respectively correspond to pyridine-like and pyrrole-like nitrogen, as illustrated in Figure S4 (Supporting Information), which contribute electron density to the π-conjugated system with a pair of p-electrons in the graphene layers. The peak at 401 eV arises when nitrogen atoms substitute carbon atoms within the graphene network and are known as "graphitic" nitrogen. It has been reported that increasing the annealing temperature results in more graphitic N incorporation into the graphene network.[14] The high energy peak at 402.2 eV is commonly attributed to oxidized nitrogen. As shown in the N1s spectrum, pyridine-like nitrogen was the main component of the N-HEG specimen. The amount of nitrogen incorporated in N-HEG was found to be about 5.9 at-%. Figures 5b and c show the high resolution

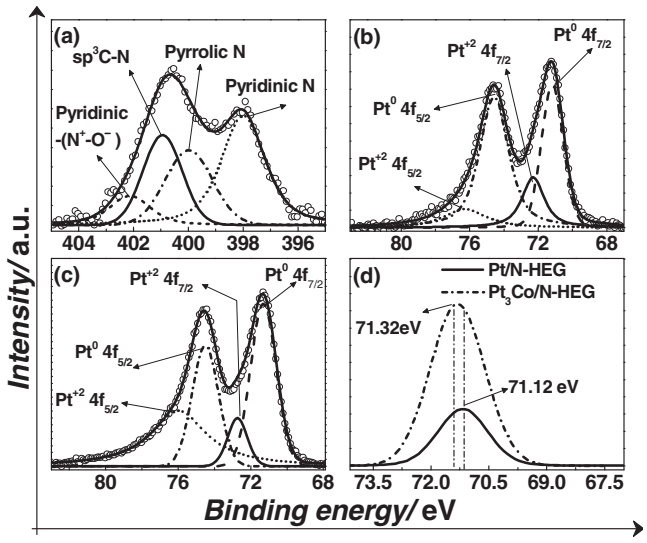

Figure 5. High resolution XPS spectra of: a) N1s orbital of N-HEG, b) Pt 4f orbital of Pt/N-HEG, and c) Pt 4f orbital of Pt_3Co/N-HEG. d) Comparison of the sub-spectra of Pt $4f_{7/2}$ corresponding to Pt^0 entities for Pt/N-HEG and Pt_3Co/N-HEG.

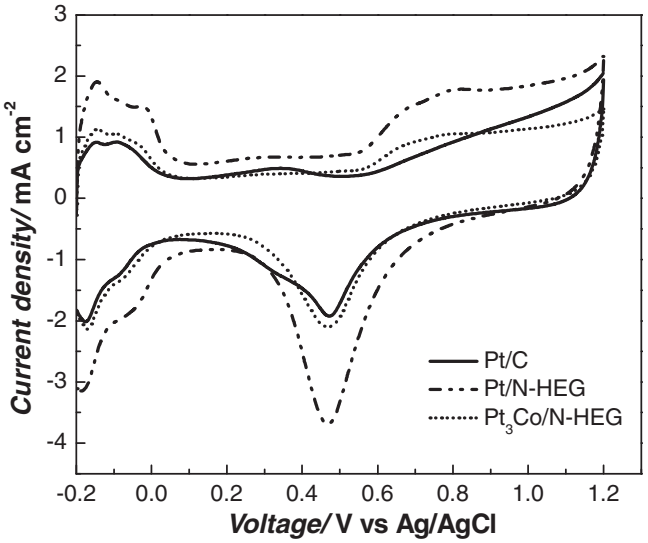

Figure 6. Cyclic voltammograms of: a) E-TEK Pt/C, b) Pt/N-HEG, and c) Pt_3Co/N-HEG.

Pt 4f XPS spectra for Pt/N-HEG and Pt_3Co/N-HEG. The Pt 4f spectrum of Pt/N-HEG was deconvoluted into four peaks. The two main peaks with binding energy (E_b) values of 71.12 and 74.58 eV arise due to the spin-orbit split doublet of Pt $4f_{7/2}$ and $4f_{5/2}$ present in the zero-valent metallic state, respectively. Two more peaks located at E_b values of 72.16 and 75.55 eV indicate the presence of oxide, wherein the Pt exists in the +2 oxidation state. In Pt_3Co/N-HEG specimen also two chemically different Pt entities could be identified, as marked in the spectrum corresponding to metallic Pt^0 with E_b of 71.32 and 74.62 eV and oxide Pt^{+2} with E_b of 72.74 and 75.99 eV, respectively. The Pt species in the monometallic Pt and binary Pt–Co alloyed nanoparticles were predominantly in the zerovalent state. For comparison, the subspectra of Pt $4f_{7/2}$ corresponding to Pt^0 entities for Pt/N-HEG and Pt_3Co/N-HEG are shown together in Figure 5d. A positive shift of about 0.2 eV for Pt_3Co (E_b approximately 71.32 eV) with respect to Pt/N-HEG (E_b approximately 71.12 eV) was observed. This binding energy upshift of about 0.2 eV is in agreement with the findings of Wakisaka et al. and confirm the influence of Co on the electronic structure of Pt.[15] This shows that Co predominantly influences the electronic structure of Pt. Some theoretical studies have reported that after alloying Pt with 3d TM atoms, the total number of electrons per Pt atom increases but that in 5d orbitals decreases because of the vacant d orbitals of the alloying element. This increase in the vacancy of Pt 5d orbital due to alloying is compensated for by an initial donation of electrons from the 2π molecular orbital of oxygen to Pt 5d orbital, which, in turn, leads to a back-donation of electrons from Pt 5d orbital to $2\pi^*$ orbital of oxygen.[16] This process of electron donation and back-donation results in an increased interaction between Pt and oxygen atoms and helps in weakening and finally the splitting of the O–O bond, thereby making the oxygen atoms available for the ORR.[16,17] In this way, alloying Pt enhances the catalytic activity of the catalysts. The high-resolution C1s XPS spectrum of N-HEG sample and Co 2p in case of Pt_3Co/N-HEG sample are shown in Figure S5 of the Supporting Information. From XPS analysis also, the Pt/Co ratio was observed to be 3:1.

The results of cyclic voltammetry (CV) of commercial E-TEK Pt/C, Pt/N-HEG, and P_3Co/N-HEG are shown in **Figure 6**. The coulombic charge for hydrogen desorption (Q_H) was used to calculate the active platinum surface of the electrodes. The electrochemical active surface area (ECSA) was calculated using the relation

$$\text{ECSA} = Q_H/[\text{Pt}] \times 0.21 \quad (1)$$

where, [Pt] represents the loading of Pt and 0.21 mC cm^{-2} is the charge required to oxidize a monolayer of H_2 on the Pt site.[18] The ECSA of the Pt/C, Pt/N-HEG, and Pt_3Co/N-HEG were obtained as 42.1, 57.9, and 48.5 $m^2\ g^{-1}$, respectively. The decrease of ECSA with Co alloying is a common phenomenon, which might be caused by the presence of Co on the particle surface that decreases the number of active Pt sites.[4] The larger ECSA for Pt/N-HEG compared with commercial Pt/C was attributed to the higher dispersion of Pt in the former sample because of the nitrogen incorporation. The present ECSA values for Pt/N-HEG and P_3Co/N-HEG are comparable or higher than those reported ECSA values for Pt/nitrogen-doped multiwalled carbon nantubes (N-MWNTs, 54.9 $m^2\ g^{-1}$) and P_3Co/N-MWNTs (41.4 $m^2\ g^{-1}$).[4]

Figure 7a,b shows the polarization curves with the cathode containing Pt/N-HEG and Pt_3Co/N-HEG electrocatalysts and anode containing commercial Pt/C electrocatalysts acquired at three different temperatures (40, 50, and 60 °C) without any back pressure. Fuel cell performances of different cathode electrocatalysts operating at 60 °C without any back pressure are shown in **Table 1**. PEMFCs with commercial Pt/C and Pt_3Co/C as cathode electrocatalysts showed a current density of 276 and 346 mA cm^{-2} at 0.6 V at 60 °C without any back pressure, as shown in Figure S6 in the Supporting Information. Among the

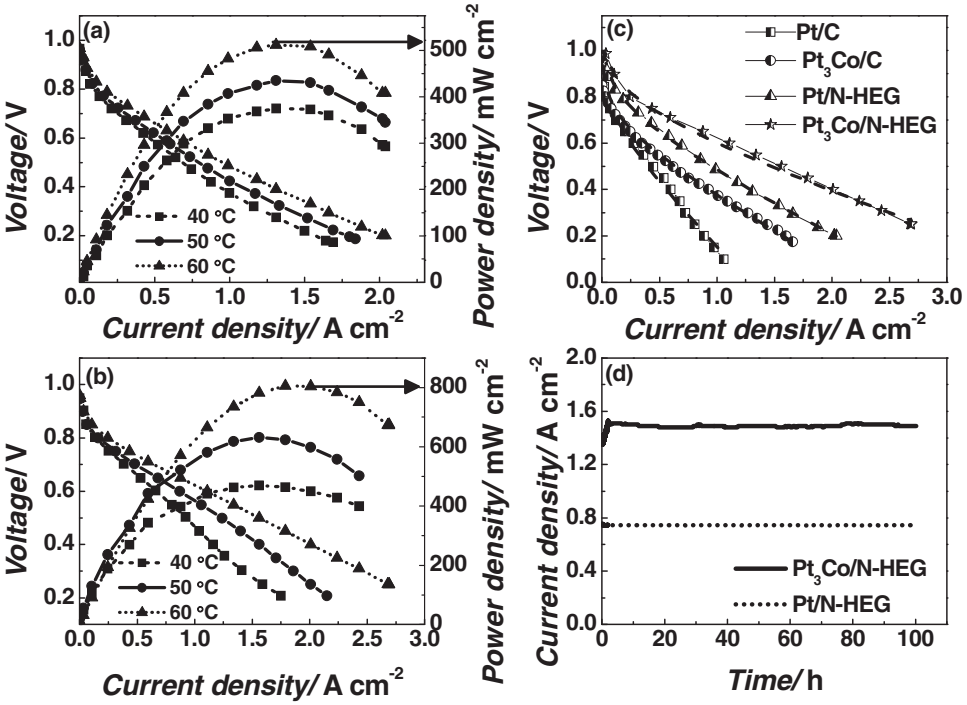

Figure 7. Polarization curves of cathode electrocatalysts: a) Pt/N-HEG and b) Pt_3Co/N-HEG with Pt/C as the anode electrocatalyst at three different temperatures (40, 50, 60 °C) without any back pressure. c) Theoretical fit of the polarization data for Pt/C, Pt_3Co/C, Pt/N-HEG, and Pt_3Co/N-HEG using Equation 2 at 60 °C. d) Stability study of the PEMFC with cathode electrocatalyst containing Pt/N-HEG and Pt_3Co/N-HEG at 60 °C without any back pressure.

cathode electrocatalysts, Pt/N-HEG and Pt_3Co/N-HEG show higher performance than commercial E-TEK Pt/C electrocatalyst, with respective current densities of 665 and 1110 mA cm^{-2} at 0.6 V, which are 2.41 and 4 times higher than that of the performance of the commercial Pt/C electrocatalyst. The maximum power densities exhibited by commercial Pt/C, commercial Pt_3Co/C, Pt/N-HEG, and Pt_3Co/N-HEG cathode electrocatalysts are 241, 379, 512, and 805 mW cm^{-2}, respectively. In addition to the commercial catalysts, the performance of Pt/N-HEG and Pt_3Co/N-HEG investigated in this work was also compared with similar types of cathode electrocatalyst. For instance, in the case of chemically reduced Pt-graphene cathode electrocatalyst, Si et al. have reported a maximum power density of about 250 mW cm^{-2} at 65 °C, while Seger et al. achieved a value of 161 mW cm^{-2} at 60 °C.[19] In the case of ORR studies of Pt–Co alloy on carbon supports, Kadirgan et al. have reported a power density value of approximately 470 mW cm^{-2} at 70 °C for Pt–Co/C as cathode catalyst.[20]

The superior performance exhibited by Pt_3Co/N-HEG cathode electrocatalyst in this work can be viewed from two perspectives, namely: i) the role played by nitrogen-doped graphene support and ii) the catalytic activity of Pt_3Co alloy nanoparticles. As discussed above, the incorporation of nitrogen atoms in the graphene network strengthens the interaction between the catalyst nanoparticles and the support, which not only helps in a better dispersion of nanoparticles on the graphene support but also averts their self-agglomeration by stabilizing them on it.[10,21] More significantly, the nitrogen doping introduces atomic charge density and asymmetry in spin density on graphene network that facilitates the charge transfer from the carbon support to the adsorbing oxygen molecule and results in the formation of superoxide ion (O^-_2).[22] This weakens the O–O bond and promotes its dissociation, thereby enhancing the ORR activity. The higher PEMFC performance of the Pt/N-HEG catalyst as compared to commercial Pt/C and Pt_3Co/C catalysts clearly establishes the importance of nitrogen doping. In the case of Pt_3Co alloy nanoparticles, the alloying of Pt with Co increases the d-vacancy of Pt, which augments the adsorption of O_2^- by a phenomenon called back-donation, which helps in the easy dissociation of the O–O bond. Also, depending upon whether a Pt atom is bonded to another Pt atom or a Co atom, the electronic structure of the primary Pt atom undergoes a change. The changed electronic structure of Pt as a result of Co alloying reduces the fractional coverage of OH species on Pt surface, thereby creating more Pt active sites for ORR; thus, faster kinetics are exhibited.[4,23]

The kinetic parameters of the polarization data were evaluated by fitting the experimental data to the semi-empirical equation[24]

$$E_{cell} = E_0 - b\log(i) - Ri \quad (2)$$

where, E_{cell} is the cell potential; E_0 is a constant, which is dependent on the cell operating conditions and the cathode electrocatalyst; b is the Tafel slope for oxygen reduction; R is the dc resistance; and i is the current density; the values are listed in Table 1. The polarization data at 60 °C were fitted to the above equation by a non-linear least-squares method in order

Table 1. Fuel cell performance of the different cathode electrocatalysts with Pt/C as anode electrocatalyst at 60 °C without any back pressure. Tafel slope and resistance values determined from theoretical fit of the data using Equation 2.

Cathode electrocatalyst	Current density at 0.6 V [mA cm^{-2}]	Maximum power density [mW cm^{-2}]	Tafel slope *b* [mV per decade]	Resistance *R* [Ω cm^2]
Pt/C	276	241	72	0.46
Pt_3Co/C	346	379	66	0.28
Pt/N-HEG	665	512	70	0.22
Pt_3Co/N-HEG	1110	805	69	0.16

to evaluate the kinetic parameters of the different electrocatalysts, which are shown in Figure 7c. All electrocatalysts display the Tafel slopes for oxygen reduction reaction in the range 65–75 mV $decade^{-1}$, in accordance with previous reports.[25] Also, PEMFC with Pt_3Co/N-HEG cathode electrocatalyst shows the lowest dc resistance (0.16 Ω cm^2) when compared with the other electrocatalysts.

The stability of Pt/N-HEG and Pt_3Co/N-HEG cathode electrocatalysts was studied by running the membrane electrode assembly (MEA) assembled with Pt/C anode electrocatalyst for 100 h at a voltage of 0.5 V at 60 °C without any back pressure (Figure 7d). The MEAs with Pt/N-HEG and Pt_3Co/N-HEG as cathode electrocatalysts deliver a current density of 750 and 1500 mA cm^{-2} at 0.5 V for 100 h without any degradation in the performance, which shows the high stability of the electrocatalysts. Doping of graphene sheets with nitrogen atoms results in strong binding between catalyst nanoparticles and graphene surface, which prevents the detachment of catalyst nanoparticles from the graphene support and their agglomoration during cell operation, thereby increasing its long-term stability. Therefore, the study shows that both electrocatalysts give very good stability along with high current density.

3. Conclusions

A novel method for uniform coating of conductive polymers, such as polypyrrole, over graphene surface was developed using an anionic polyelectrolyte. Nitrogen doping of graphene was achieved by the pyrolysis of PPy-modified graphene nanocomposite. Pt and Pt–Co alloy nanoparticles were uniformly dispersed over the nitrogen-doped graphene by the modified-polyol reduction method and their electrocatalytic activity towards the ORR were studied by PEMFC full cell measurements. At 60 °C, the Pt/N-HEG and Pt_3Co/N-HEG cathode electrocatalysts yielded a maximum power density of 512 and 805 mW cm^{-2}, respectively, without applying any back pressure. The high power density exhibited by Pt_3Co/N-HEG, which is about four times higher than that of commercial Pt/C cathode electrocatalyst, is attributed to the combined effects of the modified Pt state due to alloying and nitrogen doping, uniform dispersion of catalyst nanoparticles, and high catalytic activity of the N-HEG support itself. The stability study shows that Pt_3Co/N-HEG cathode electrocatalyst is highly durable in acidic medium due to the strong binding between metal nanoparticles and nitrogen-modified graphene, which prevent the agglomeration of catalyst nanoparticles. The study demonstrates two promising electrocatalysts for PEMFC applications, which on the basis of performance and stability present the possibility of replacing contemporary electrocatalysts.

4. Experimental Section

Materials: The materials used included ethylene glycol (EG, Merck), sodium chloride (NaCl, Aldrich), poly(sodium 4-styrenesulfonate) (PSS, MW = 70 000, Aldrich), pyrrole monomer (Aldrich), hydrochloric acid (HCl, Aldrich), ferric chloride ($FeCl_3.6H_2O$, Aldrich), hexachloroplatinic acid ($H_2PtCl_6{\cdot}6H_2O$, Aldrich), cobalt nitrate ($Co(NO_3)_2.6H_2O$, Aldrich), and Nafion solution (5% in isopropanol and water). Graphite oxide powder was used as-synthesized. Deionized (DI) water was used in all synthesis procedures.

Synthesis of Nitrogen-Doped Graphene: GO was prepared from purified natural graphite using Hummers' method.[26] Graphene was synthesized by the hydrogen exfoliation method.[27] Briefly, GO was taken in a quartz boat and placed inside a tubular furnace. The furnace was sealed at both the ends with end couplings having provision for gas flow. The furnace was flushed with Argon (99.99%) for 15 min. The temperature of the furnace was then raised to approximately 200 °C. Very pure hydrogen gas (99.99%) was introduced at this temperature. Exfoliation occurred within 1 min, which was easily visible. This HEG was wrapped with the PSS polyelectrolyte by following the method reported by Yang et al.[28] HEG was dispersed in a aqueous solution (1 wt%) of anionic PSS polyelectrolyte (0.15 mg mL^{-1}) by a combination of strong stirring and sonication. The solution was then stored at 50 °C for 12 h. The final solution was then filtered and washed several times to remove the excess PSS in the solution followed by drying in a vacuum oven at 70 °C for 24 h.

Polypyrrole was coated on PSS modified HEG (PHEG) by chemical polymerization of pyrrole (0.5 mL) with $FeCl_3$ (1.2 g) in HCl solution (50 mL of 0.1 mol L^{-1}). The final materials were then filtered and washed with a large amount of water and subsequently with ethanol to remove the residual oxidant. Finally, all composites were washed with acetone and dried at 60 °C to obtain PPy–PHEG. Next, PPy–PHEG was heated at 800 °C in an argon atmosphere in order to remove all the polymer from the graphene surface and incorporating nitrogen atoms in the graphene network, yielding N-HEG.

Chemical Reduction for Loading of Pt and Pt_3Co over Nitrogen-Doped Graphene: Pt and Pt–Co alloy nanoparticles were decorated on N-HEG by the modified-polyol reduction method. For that, N-HEG (100 mg) was dispersed in a mixture of EG and water (200 mL) by ultrasonication and followed by stirring. Appropriate amounts of $H_2PtCl_6.6H_2O$ and $Co(NO_3)_2.6H_2O$ solutions were added to the suspension drop-wise and stirred for 12 h. To get Pt_3Co alloy nanoparticles, the molar ratio of Pt and Co in the suspension was adjusted to 3:1. The pH of the entire solution was adjusted to 11 by adding NaOH (2.5 M) and the solution was refluxed at 130 °C for 7 h to ensure that all the Pt and Co were completely reduced. The water to EG ratio was controlled at 1:3

throughout the reaction. Finally, the solution was filtered and the final product was washed with DI water and dried at 70 °C for 8 h in a vacuum oven. The final products were labeled as Pt_3Co/N-HEG and Pt/N-HEG.

Material Characterization: The X-ray diffraction measurements were performed in a PANalytical X'Pert Pro X-ray diffractometer with nickel-filtered Cu K_α radiation as the X-ray source. The pattern was recorded in the 2θ range of 5° to 90° with a step size of 0.016°. The vibrational characteristics of the samples were analyzed via Raman spectroscopy using a 532 nm laser (Witec Alpha 300) as the excitation source in the range 100–3000 cm^{-1}. The morphology of the samples was characterized by field emission scanning electron microscopy (FEI QUANTA 3D), and transmission electron microscopy (FEI Tecnai G^2 20 S-TWIN, 200 keV). Energy dispersive X-ray analysis was carried out in FESEM equipped with a Li-doped silicon X-ray detector. X-ray photoelectron spectroscopy (Omicron Nanotechnology) was used to determine the oxidation state of various elements present in the samples. Functional group identification was done using a PERKIN ELMER FTIR spectrometer in the range 400–4000 cm^{-1} using the KBr pellet method.

Cyclic Voltammetry: Cyclic voltammetry studies were carried out in a three-electrode electrochemical cell (CHI 608C instrument) to determine the electrochemical active surface area. The working electrode was prepared by mixing the electrocatalyst (5 mg) with Nafion (5 wt%, 5 μL) and ethanol (200 μL) and sonicating the solution for 10 min. A measured volume (2 μL) of this mixture was then put onto a clean and polished glassy carbon electrode substrate and dried at room temperature for 24 h. A Pt wire and Ag/AgCl were used as counter and reference electrodes, respectively, and all scanning of the potential was done from –0.2 to 1.2 V vs. Ag/AgCl (scan rate of 50 mV s^{-1}) in H_2SO_4 (1 M).

PEMFC Single-Cell Performance Tests: The membrane electrode assembly consists of two electrodes (anode and cathode) and a polymer electrolyte. Both the anode and the cathode were made up of a backing layer, a gas diffusion layer, and a catalyst layer. The catalyst layer was prepared by uniform coating of catalyst ink over the gas diffusion layer. The catalyst ink was prepared by ultrasonicating the required amount of catalyst in DI water and propan-2-ol with 5 wt% Nafion solution. Platinum loadings of 0.25 and 0.4 mg cm^{-2} were maintained at the anode and the cathode electrocatalysts, respectively. The effective electrode area was 11.56 cm^2. The MEA was prepared by sandwiching a pretreated Nafion 212 CS membrane between the anode and the cathode by hot-pressing at 130 °C and 70 bar for 4 min. The MEAs were tested in the Teledyne fuel cell test station by fixing it between two graphite plates, which had a provision for gas flow (serpentine-type flow). The performance of the fuel cell was studied at three different temperatures (40, 50, and 60 °C) and relative humidity of 90% without any back pressure.

Supporting Information

Supporting Information is available from the Wiley Online Library or from the author.

Acknowledgements

The authors are grateful to Indian Institute of Technology Madras, Chennai, India and Intellectual Ventures, USA for filing this work as a patent.

Received: October 22, 2011
Revised: December 13, 2011
Published online: May 11, 2012

[1] a) X. Yuan, X. Zeng, H.-J. Zhang, Z.-F. Ma, C.-Y. Wang, *J. Am. Chem. Soc.* **2010**, *132*, 1754; b) A. Morozan, B. Jousselme, S. Palacin, *Energy Environ. Sci.* **2011**, *4*, 1238.
[2] H. A. Gasteiger, S. S. Kocha, B. Sompalli, F. T. Wagner, *Appl. Catal., B* **2005**, *56*, 9.
[3] a) D. V. Noto, E. Negro, R. Gliubizzi, S. Lavina, G. Pace, S. Gross, C. Maccato, *Adv. Funct. Mater.* **2007**, *17*, 3626; b) M. A. García-Contreras, S. M. Fernández-Valverde, J. R. Vargas-García, M. A. Cortés-Jácome, J. A. Toledo-Antonio, C. Ángeles-Chavez, *Int. J. Hydrogen Energy* **2008**, *33*, 6672.
[4] S. Jiang, Y. Ma, G. Jian, H. Tao, X. Wang, Y. Fan, Y. Lu, Z. Hu, Y. Chen, *Adv. Mater.* **2009**, *21*, 4953.
[5] J. Wu, X. Z. Yuan, J. J. Martin, H. Wang, J. Zhang, J. Shen, S. Wu, W. Merida, *J. Power Sources* **2008**, *184*, 104.
[6] Y. Sun, Q. Wu, G. Shi, *Energy Environ. Sci.* **2011**, *4*, 1113.
[7] R. I. Jafri, T. Arockiados, N. Rajalakshmi, S. Ramaprabhu, *J. Electrochem. Soc.* **2010**, *157*, B874.
[8] C. Zhu, S. Guo, Y. Zhai, S. Dong, *Langmuir* **2010**, *26*, 7614.
[9] Y. Shao, S. Zhang, M. H. Engelhard, G. Li, G. Shao, Y. Wang, J. Liu, I. A. Aksay, Y. Lin, *J. Mater. Chem.* **2010**, *20*, 7491.
[10] Y. Zhou, K. Neyerlin, T. S. Olson, S. Pylypenko, J. Bult, H. N. Dinh, T. Gennett, Z. Shao, R. O'Hayre, *Energy Environ. Sci.* **2010**, *3*, 1437.
[11] Y. Wang, Y. Shao, D. W. Matson, J. Li, Y. Lin, *ACS Nano* **2010**, *4*, 1790.
[12] L. Qu, Y. Liu, J.-B. Baek, L. Dai, *ACS Nano* **2010**, *4*, 1321.
[13] a) Y.-G. Zhou, J.-J. Chen, F.-B. Wang, Z.-H. Sheng, X.-H. Xia, *Chem. Commun.* **2010**, *46*, 5951; b) Z. Liu, C. Yu, I. A. Rusakova, D. Huang, P. Strasser, *Top. Catal.* **2008**, *49*, 241.
[14] Z.-H. Sheng, L. Shao, J.-J. Chen, W.-J. Bao, F.-B. Wang, X.-H. Xia, *ACS Nano* **2011**, *5*, 4350.
[15] M. Wakisaka, S. Mitsui, Y. Hirose, K. Kawashima, H. Uchida, M. Watanabe, *J. Phys. Chem. B* **2006**, *110*, 23489.
[16] S. Axnanda, K. D. Cummins, T. He, D. W. Goodman, M. P. Soriaga, *ChemPhysChem* **2010**, *11*, 1468.
[17] M. Weinert, R. E. Watson, *Phys. Rev. B* **1995**, *51*, 17168.
[18] A. Pozio, M. De Francesco, A. Cemmi, F. Cardellini, L. Giorgi, *J. Power Sources* **2002**, *105*, 13.
[19] a) Y. Si, E. T. Samulski, *Chem. Mater.* **2008**, *20*, 6792; b) B. Seger, P. V. Kamat, *J. Phys. Chem. C* **2009**, *113*, 7990.
[20] F. Kadirgan, A. M. Kannan, T. Atilan, S. Beyhan, S. S. Ozenler, S. Suzer, A. Yörür, *Int. J. Hydrogen Energy* **2009**, *34*, 9450.
[21] R. Lv, T. Cui, M.-S. Jun, Q. Zhang, A. Cao, D. S. Su, Z. Zhang, S.-H. Yoon, J. Miyawaki, I. Mochida, F. Kang, *Adv. Funct. Mater.* **2011**, *21*, 999.
[22] a) L. Zhang, Z. Xia, *J. Phys. Chem. C* **2011**, *115*, 11170; b) D. Geng, Y. Chen, Y. Chen, Y. Li, R. Li, X. Sun, S. Ye, S. Knights, *Energy Environ. Sci.* **2011**, *4*, 760.
[23] a) V. R. Stamenkovic, B. S. Mun, M. Arenz, K. J. J. Mayrhofer, C. A. Lucas, G. Wang, P. N. Ross, N. M. Markovic, *Nat. Mater.* **2007**, *6*, 241; b) L. Xiong, A. Manthiram, *J. Mater. Chem.* **2004**, *14*, 1454.
[24] E. A. Ticianelli, C. R. Derouin, A. Redondo, S. Srinivasan, *J. Electrochem. Soc.* **1988**, *135*, 2209.
[25] A. L. M. Reddy, S. Ramaprabhu, *J. Phys. Chem. C* **2007**, *111*, 16138.
[26] W. S. Hummers Jr., R. E. Offeman, *J. Am. Chem. Soc.* **1958**, *80*, 1339.
[27] A. Kaniyoor, T. T. Baby, S. Ramaprabhu, *J. Mater. Chem.* **2010**, *20*, 8467.
[28] a) W. Yang, X. Wang, F. Yang, C. Yang, X. Yang, *Adv. Mater.* **2008**, *20*, 2579; b) M. A. Correa-Duarte, N. Sobal, L. M. Liz-Marzán, M. Giersig, *Adv. Mater.* **2004**, *16*, 2179.
[29] P. Ayala, A. Grüneis, T. Gemming, B. Büchner, M. H. Rümmeli, D. Grimm, J. Schumann, R. Kaltofen, F. L. Freire Jr., H. D. F. Filho, T. Pichler, *Chem. Mater.* **2007**, *19*, 6131.
[30] H. T. Duong, M. A. Rigsby, W.-P. Zhou, A. Wieckowski, *J. Phys. Chem. C* **2007**, *111*, 13460.